UC San Diego
UC San Diego Previously Published Works

Title

Localization of nonlinear damage using state-space-based predictions under stochastic excitation

Permalink

https://escholarship.org/uc/item/8pz6z1v7

Journal

Smart Materials and Structures, 23(2)

ISSN

0964-1726

Authors

Liu, Gang
Mao, Zhu
Todd, Michael
et al.

Publication Date

2014-02-01

DOI

10.1088/0964-1726/23/2/025036

Peer reviewed

Damage detection using transient trajectories in phase-space with extended random decrement technique under non-stationary excitations

Gang Liu[1,2], Zhu Mao[3] and Michael Todd[4]

[1]Key Laboratory of New Technology for Construction of Cities in Mountain Area (Chongqing University), Ministry of Education, Chongqing, 400045, China
[2]School of Civil Engineering, Chongqing University, Chongqing, 400045, China
[3]Department of Mechanical Engineering, University of Massachusetts Lowell, Lowell, MA, 01854, USA
[4]Department of Structural Engineering, University of California San Diego, La Jolla, CA, 92093, USA

Abstract This paper proposes a damage detection method based on the geometrical variation of transient trajectories in phase-space, and the proposed methodology is compatible with non-stationary excitations (e.g., earthquake-induced ground motion). The work presented assumes zero-mean non-stationary excitation, and extends the random decrement technique to convert non-stationary response signals of the structure into free-vibration data. Transient trajectories of the structure are reconstructed via the embedding theorem from the converted free-vibration data, and trajectories are mapped successively into phase-space to enhance statistical analysis. Based upon the characterized system dynamics in terms of phase-space, the time prediction error is adopted as the damage index. To identify the presence and severity of damage in a statistically rigorous way, receiver operating characteristic curves and the Bhattacharyya distance are employed. The results from both numerical simulations and experiments validate the proposed framework, when the test structures are subject to non-stationary excitations. The extension achieved in this paper enables the phase-space damage detection approach to be compatible with non-stationary scenarios, such as traffic, wind, and earthquake loadings. Moreover, the results indicate that this phase-state-based method is able to identify damage-induced nonlinearity in response, which is an intrinsic characteristic associated with most structural damage types.

Keywords: structural health monitoring, phase-space, non-stationary excitation, random decrement technique, nonlinear damage

1 Introduction

Vibration-based damage detection techniques are widely applied to prevent structural catastrophes, optimize maintenance schedules, minimize retrofit costs, and extend remaining useful lives. Numerous nondestructive testing approaches such as ultrasonic interrogation, X-ray radiography, eddy current, and thermal imaging have been developed and utilized for the past decades. However, the aforementioned techniques are primarily local detection approaches and impractical, even impossible, to implement for inaccessible components or large-sized structures [1-3]. As an alternative, vibration-based structure health monitoring (SHM), which

has flourished in recent years, provides an effective and reliable approach for identifying globally-observant ("performance level") damage in aerospace, mechanical, and civil structures.

One major category of processing vibration-based SHM testing measurements algorithm is driven by data analytics, in which damage features are directly extracted from the measured structural responses [4]. In such data-driven modeling, prior assumptions on physics-based modeling and intensive forward computation of their subsequent model evaluations are bypassed, which makes them enjoy broader applicability in SHM [5]. Recent successful examples include autoregressive, autoregressive/moving average, wavelet, Hilbert–Huang transform, and network-based data modeling methods [4].

In recent years, a novel data-driven damage detection method, rooted in reconstructing the system's phase-space, has been proposed based on characterizing geometric variation of steady-state dynamics [6-9]. Under deterministic (and originally, chaotic) excitation, the attractor is reconstructed from observed steady-state structural responses according to the principles of embedology, and then relevant damage features are extracted from topology changes of the attractor between the baseline and test conditions, which are formally compared under hypothesis testing. It has been reported that the damage detection resolution of this method is of an order-of-magnitude higher than several conventional data driven model-based methods [10]. Moreover, the phase-space methodology is able to identify damage-induced nonlinearity, which is an intrinsic characteristic associated with many damage types such as bolt loosening and breathing cracks [11].

One issue critical to this phase-space-based method is the application of chaotic excitation (for sufficient phase/frequency diversity in response) to extract damage features from the steady-state response. This is sometimes impractical or implausible for complex, spatially-extended structures with large dimension and complexity, such as high-rise buildings and aerospace vehicles. Although Nichols et al., Overbey et al., and Gang et al. have shown that phase-space embedding may be employed practically for structural damage detection even with stationary stochastic excitations [12-15], most ambient excitations encountered in the real world are non-stationary in nature, e.g., traffic loading, fluctuating wind loading, and seismic waves. Therefore, it is desirable to develop an applicable phase-state-based approach for non-stationary excitations.

Considering the fact that transient trajectories reconstructed from the free response of a structure conveys damage-induced information, a new method is proposed to detect damage under non-stationary excitations. In lots of the realistic applications, the non-stationarities fall into a weak form, i.e. the higher order statistics are time-dependent but the mean stays constant. For instance, the ambient excitations from earthquake, wind, traffic, etc. are all feasibly modeled as constant (zero) mean series in numerous literatures. This work extends the traditional random decrement technique, for free decay responses with stationary excitations, to the scenarios with non-stationary structural responses, by assuming zero-mean non-stationary excitations. Multiple reconstructed trajectories from free decay responses are overlapped in order to enhance the data points for a statistical analysis. The time prediction algorithm is employed to extract the damage feature from transient trajectories obtained from the baseline and testing conditions. The receiver operating characteristic (ROC) curve and the Bhattacharyya distance are adopted as statistical tools to identify the presence and severity of the damage. To validate the proposed flow, a 3-degree-of-freedom numerical model with both

linear and nonlinear damages is introduced, as well as an experimental test-bed with bolt-loosening damage. Excited by non-stationary time series, both the linear and nonlinear damages can be detected in the numerical verification example. For the experimental test-bed, the nonlinear damages induced by loosened bolts are also identified successfully. The rest of this article is organized as this: section 2 introduces the traditional random decrement technique and extents it to non-stationary excitation, section 3 proposes the novel damage detection method using transient trajectories, section 4 and section 5 explore a numerical and experimental example to verify the proposed method respectively, and section 6 gives the conclusion.

2 Extended random decrement technique

2.1 Random decrement technique

The original random decrement (RD) technique was introduced by Henry Cole in the early 1970s for estimating damping in aerospace structures [16]. Generally, given initial displacement, velocity, and random excitation, the "randomdec" signatures of the system can be extracted from the measured response $x(t)$ using RD function $\delta(p)$ estimated as [17]:

$$\widehat{\delta}(p) = \frac{1}{N} \sum_{k=1}^{N} \{x(t_k + p) \mid x(t_k) = A\}, \qquad (1)$$

where A is the "initial condition" value assumed by $x(t)$ at time t_k, p is the forward time window comprising the response range $x(t_k{:}t_k{+}p)$ initiated from time t_k, and N is the number of such p-windows. The implement of the RD function is straightforward and demonstrated in Figure 1.
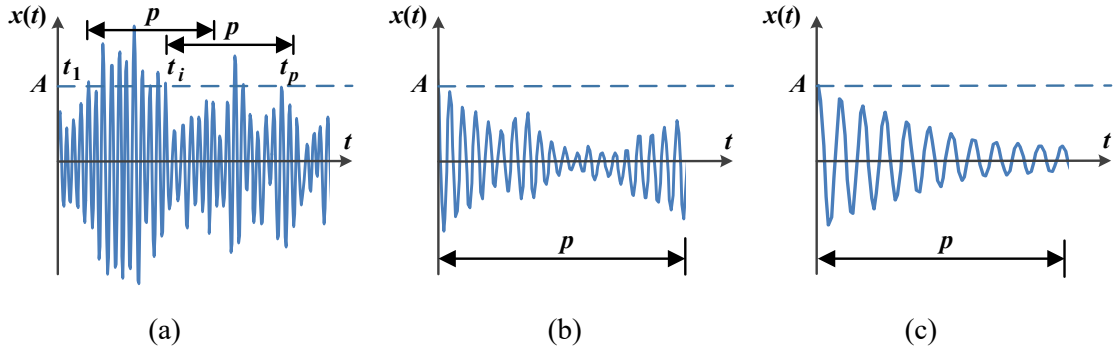
Figure 1. Procedure of RD technique for (a) original response (b) RD after several averages, and (c) RD after sufficient number of averages

Using Eq. (1), the randomdec signature of linear structures is composed of two parts. The first part contributing the randomdec signature is the transient part, which is determined by initial conditions. Since all sections begin with the same initial condition A, the transient part obtained from the RD technique is the free decay response of the system. On the other hand, the second part is the "steady state" part (the particular solution) dependent upon the random excitations. With sufficient averaging, the random part will vanish, leading to only the transient free decay response in the randomdec signature. Therefore, the randomdec signature under stationary excitation is of the same form with the free decay response of the system.

2.2 Extended random decrement technique

In theory, the aforementioned RD technique requires stationary excitation; however, most ambient excitation is non-stationary in nature. So it is necessary to extend the RD technique to non-stationary processes, which is more general for mechanical and civil structures.

Considering a multi-degree-of-freedom linear system subjected to zero-mean non-stationary excitation $f(t)$, the equation of motion can be expressed as,

$$M\ddot{x} + C\dot{x} + Kx = f(t),\tag{2}$$

where M, C and K are the mass, damping and stiffness matrix respectively, x is the displacement response, and $\dot{x}$ and $\ddot{x}$ are the time derivatives for different orders, i.e. velocity and acceleration. According to the dynamics for linear structures, the displacement response at the i-th degree-of-freedom can be defined as,

$$x_i(t) = \sum_{r=1}^{m} \varphi_{ir} Y_r(t),\tag{3}$$

where φ_{ir} denotes the value of the r-th modal vector at the i-th degree, m is the modal order and $Y_r(t)$ describes the r-th modal displacement. Substituting Eq. (3) into Eq. (1), the RD function can be rewritten as

$$\hat{\delta}_i(p) = \frac{1}{N}\sum_{k=1}^{N}\sum_{r=1}^{m}\varphi_{ir}Y_r(t_k+p) = \sum_{r=1}^{m}\varphi_{ir}\left\{\left(\frac{1}{N}\sum_{k=1}^{N}Y_r(t_k+p)\right)\Bigg|\sum_{r=1}^{m}\varphi_{ref,r}Y_r(t_k)=A\right\},\tag{4}$$

where subscript *ref* denotes the reference degree-of-freedom. According to dynamics of structures, the r-th model displacement is the addition of two parts,

$$Y_r(t) = Y_{r1}(t) + Y_{r2}(t),\tag{5}$$

where

$$Y_{r1}(t) = \left[Y_r(0)\cos(\omega_{Dr}t) + \frac{\dot{Y}_r(0) + Y_r(0)\xi_r\omega_r}{\omega_{Dr}}\sin(\omega_{Dr}t)\right]e^{-\xi_r\omega_r t},$$

$$Y_{r2}(t) = \int_0^t \varphi_r^T f(\tau)g_r(t-\tau)d\tau\tag{6}$$

and ξ_r, ω_r and ω_{Dr} are the r-th modal damping ratio, natural frequency and damping frequency respectively. $Y_r(0)$ and $\dot{Y}_r(0)$ are the initial modal displacement and velocity for the r-th model respectively. $g_r(t\text{-}\tau)$ denotes the unit impulse response function of the linear structure system. Because the unit impulse response function attenuates, it is assumed that the "influence time" of this function is limited, thus $Y_{r2}(t)$ can be rewritten as,

$$Y_{r2}(t) = \int_0^t \varphi_r^T f(\tau)g_r(t-\tau)d\tau = \int_0^q \varphi_r^T f(t-\tau)g_r(\tau)d\tau,\tag{7}$$

where q describes the length of the unit impulse response function. Substituting t with t_k+p in Eq. (5) and Eq.(6), there is

$$Y_r(t_k+p) = \left[B_{r,t_k}\cos(\omega_{Dr}p) + C_{r,t_k}\sin(\omega_{Dr}p)\right]e^{-\xi_r\omega_r p} + \int_0^q \varphi_r^T f(t_k+p-\tau)g_r(\tau)d\tau,\tag{8}$$

where

$$B_{r,t_k} = \left(Y_r(0)\cos\omega_{Dr}t_k + \frac{\dot{Y}_r(0) + Y_r(0)\xi_r\omega_r}{\omega_{Dr}}\sin\omega_{Dr}t_k\right)e^{-\xi_r\omega_r t_k}$$

$$C_{r,t_k} = \left(-Y_r(0)\sin\omega_{Dr}t_k + \frac{\dot{Y}_r(0) + Y_r(0)\xi_r\omega_r}{\omega_{Dr}}\cos\omega_{Dr}t_k\right)e^{-\xi_r\omega_r t_k}.$$

The Appendix provides the detailed calculation of randomdec signal $F(p)$ of non-

stationary excitation and the corresponding statistical properties. Substituting the calculated $F(p)$ and Eqs. (5-8) into Eq. (4), the RD function can be expressed as,

$$\hat{\delta}_i(p) = \sum_{r=1}^{m} \varphi_{ir} G(p) + \sum_{r=1}^{m} \varphi_{ir} \int_0^q \varphi_r^T g_r(\tau) \frac{1}{N} \sum_{k=1}^{N} f(t_k + p - \tau) d\tau$$
$$= \sum_{r=1}^{m} \varphi_{ir} G(p) + \sum_{r=1}^{m} \varphi_{ir} \int_0^q \varphi_r^T g_r(\tau) F(p) d\tau$$

where

$$G(p) = e^{-\xi_r \omega_r p} \left(\left(\frac{1}{N} \sum_{k=1}^{N} B_{r,t_k} \right) \cos \omega_{Dr} p + \left(\frac{1}{N} \sum_{k=1}^{N} C_{r,t_k} \right) \sin \omega_{Dr} p \right)$$

From Eq. (9), if the system is subjected to non-stationary excitation with zero mean, the random decrement signature of system response includes two terms. The first term is only relative to the initial modal displacement and velocity of the linear system, which is equivalent to the free decay responses of the system. The second term in Eq. (9) depends on the external excitation. According to the detailed derivation and discussion given in Appendix, the mean of $F(p)$ is zero and the variance of $F(p)$ converges to zero quadraticly as the superimposed time N increases; thus the second term should be close to 0 or negligible as noise in engineering practice. So the randomdec signatures of a system subjected to non-stationary excitation are of the same form as free vibration decay of the structure. Therefore, the original RD technique is extended to deal with non-stationary excitation, which is called extended random decrement technique (ERD) in this paper.

Based on the superposition principle, application of the ERD technique requires the assumption of structural system linearity. However, the random decrement technique has been successfully employed to nonlinear systems by several studies, such as estimation modal parameters for the nonlinear roll motion equation [18] and damage detection for nonlinear dynamic systems [19]. Consequently, ERD technique can be reasonably extended to extract free decay response for nonlinear structures.

3 Damage identification method

3.1 Trajectories reconstruction

A d-dimension dynamic system may be described by the first-order ordinary differential equation,

$$\dot{\xi} = \Gamma(\xi, t), \; \xi \in R^d, \tag{10}$$

where ξ is the state vector and Γ is a generic/nonlinear function of the state variables and time t, and $\dot{\xi}$ describes the first-order derivative of state variable with respect to time. Regarding each dimension of the state vector as an independent coordinate, the state vector, as a function of time, forms trajectories in the phase state. It is usually impractical to measure all the state variables during experiments, but according to the embedding theorems proposed by Takens [20], the qualitative trajectory can be reconstructed from a single measured variable. That is to say, the single measured time series are copied n times in an appropriately delayed fashion, in order to represent the n coordinates of the reconstructed trajectory. Hence, each discrete time instance of the trajectory at time l can be expressed as

$$\Xi(l) = [\xi(l), \xi(l+T), ..., \xi(l+(n-1)T)],\qquad\qquad(11)$$

where T is the time lag (delay) and n is named embedding dimension. The geometric shape of the trajectory depends on embedding parameters T and n. If the lag is selected too small, such as $T = 0$, the reconstructed trajectory will be identical to each other, so that there is no redundant information. However, for overly long lags, the resulting trajectory will become temporally unrelated, and thus the underlying dynamics of the trajectory will be destroyed. While there is no single optimal lag, one strongly-motivated choice may be obtained in accordance with choosing a minimum in the average mutual information (AMI) function[21], which indicates there is little statistical redundancy in the time series at that corresponding lag. The common criterion is to select the value T when the AMI function reaches its first minimum.

Moreover, improper choice of the embedding dimension n may also lead to a poor reconstruction. When the dimension is chosen too small, the trajectory may intersect itself, while large n will result in computational burdens (the "curse of dimensionality") and possibly embedding external randomness, i.e, non-causal dynamical response. A frequently used algorithm for optimal choice of n is the false nearest neighbors (FNN) approach [22], in which the trajectory is embedded in $n=1$ dimensions, the nearest neighbors to each point in the trajectory are determined. Then the trajectory is successively embedded in higher and higher n values while the percentage of false projections of the nearest neighbors is calculated. The percentage of false nearest neighbors should decline to zero or at least a very small value if the trajectory is considered fully unfolded. Thus, the dimension corresponding to the first zero percentage of FNN is chosen as the optimal (minimal) embedding dimension.

3.2 The damage feature and damage detection metric

Under chaotic excitation, the trajectory of a dynamic system will asymptotically migrate toward the steady-state condition (i.e., the attractor), which is a deterministic object. Therefore, the trajectory can be utilized to identify damages. Similarly, since the signal from ERD technique asymptotically decreases from initial condition toward zero along specific trajectory, the transient trajectory is a deterministic process and may be utilized as a candidate feature for damage detection.

Using the reconstructed transient trajectory, statistically averaged features may be developed to capture the spatial or temporal evolution of points on the baseline trajectory as a predictor for how points will evolve on a testing trajectory. Since the baseline and testing trajectory are both decayed from the initial condition to nearly zero, they can be viewed as measurement synchronization, thus the time prediction strategy is utilized in this work [9]. For time prediction algorithm, two fiducial points $\xi(t)$ and $\zeta(t)$ at the same time index t are randomly selected from baseline trajectory Ξ and test trajectory Z respectively. And then the nearest geometrically corresponding neighborhoods are acquired for each fiducial point, giving

$$z_{nnf}(q_j): |q_j - s| > h, \qquad j = 1,2,...,Q,\qquad\qquad(12)$$

where h denotes a Theiler window, the subscript nnf refers to the nearest neighbors, z denotes ξ or ζ, and Q is the number of neighbors. In order to minimize artificial near-time correlations, the Theiler window is used to separate the neighbors whose time index q_j to s is closer than h steps. Parameter h usually is a function of the time lag and $h = 2T$ is adopted in this study.

Next, each neighbor set is time-incremented L time steps (time prediction horizon) in the future and the time prediction error is quantified by the Euclidean distance between the centroid of time-evolved neighbor set on these two trajectories:

$$\text{TPE}_s = \left\| \overline{\zeta}_{s+L,q_j} - \overline{\xi}_{s+L,q_j} \right\|, \tag{13}$$

where TPE_s is the point-wise time prediction error for a given fiducial point. A schematic of time prediction algorithm is illustrated in Figure 2.

| (a) | (b) |
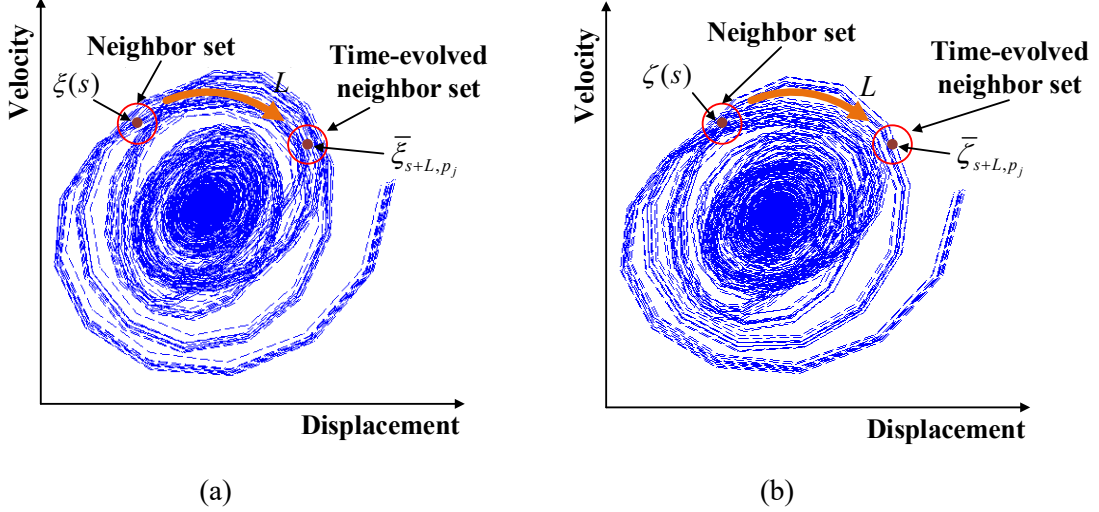
Figure 2. Time prediction strategy for (a) baseline trajectory X (b) testing trajectory Y

Then, a set of fiducial points are randomly selected, and their TPEs are computed. Because the distribution of the TPE, a random variable, is usually unknown, the bootstrap technique is adopted to resample the TPE, resulting in a time prediction error mean (TPEM) [23]. According to central limit theorem, the distribution of TPEM is reasonably assumed to be normal due to the averaging, and TPEM is used as the damage feature in this study.

The transient trajectory is reconstructed from the structural free decay response, thus it approaches the origin within a few recurrences in the phase state. Correspondingly, if there are insufficient neighbors for statistical analysis, or the radius for searching neighbors is too large to explore the local dynamics, the damages cannot be identified accurately. An overlapping strategy is adopted to overcome this limitation. The structural response is divided into k segments with the same length. After a free decaying vibration corresponding to one segment is calculated by the ERD technique, it will be reconstructed into the same phase state overlapping with the other k-1 trajectories.

The number of fiducial points ξ and the number of neighbors Q depend on the total number of points in the phase–state, if damage features are extracted from steady-state trajectory. However, in this study, the trajectories are transient, thus ξ and Q no longer obey this rule. Instead, ξ should be related to the number of points on the trajectory before overlapping, due to the similarity of those overlapped trajectories from the same initial condition, and the number of neighbors Q should depend on the number of the trajectories. Without losing generality, ξ is arbitrarily set to be half of the number of points on the trajectory in this work, and Q is set to be half of the number of trajectories k. A parametric study is carried out later in this paper.

With transient trajectories reconstructed, prediction errors from both baseline and testing conditions are available as two clusters. With the distributions described probabilistically, the

area under the receiver operating characteristic curves (AUC) and the Bhattacharyya distance (BD) are introduced to detect the presence and magnitude of damages in a statistically significant sense. The ROC curve is a visualization depicting the true positive rate (as vertical axis) against the false positive rate (as horizontal axis) for all possible classifications. The ROC curve with high true positive rate and low false positive rate, will locate at upper right corner in the figure. Hence, when the area under ROC curve approaches 1, perfect classification is achieved, and when its value is 0.5, classification performance is equivalent to a random guess [14].

The BD is a statistical distance measured defined as [24]

$$BD = \frac{1}{4}\frac{(u_d - u_h)^2}{\sigma_d^2 + \sigma_h^2} + \frac{1}{2}\ln\left[\frac{(\sigma_d^2 + \sigma_h^2)/2}{\sigma_d \sigma_h}\right], \tag{14}$$

where u and σ correspond to the means and standard deviations of TPEM for baseline and testing (damaged) conditions. The subscripts h and d represent the baseline and damaged condition respectively. If the value of σ_h and σ_d are the same, the second term becomes zero, and the BD reduces to the conventional definition of Fisher exponent or deflection coefficient. Compared to traditional statistical distance measures, the BD better encodes the separation of distributions under different damage scenarios; if the damage primarily causes change of variances instead of a mean shift, the BD evaluation is dominated by the second term, which cannot be represented in the conventional Fisher distance. The procedure of the proposed method is plotted in Figure 3.

As damage level progressively increases, the TPEM distributions will correspondingly deviate along one side apart from the distribution of the baseline. But due to the uncertainty of ambient excitation, damage does not move the TPEM distribution monotonically when the structure is in a low-level damage condition. In order to reduce the uncertainty, if the TPEM distribution locates at the opposite side, the AUC is set to be 0.5 and BD is set to be 0.001 artificially, indicating the classification result is vague and there is no detectable damage affecting the global performance.
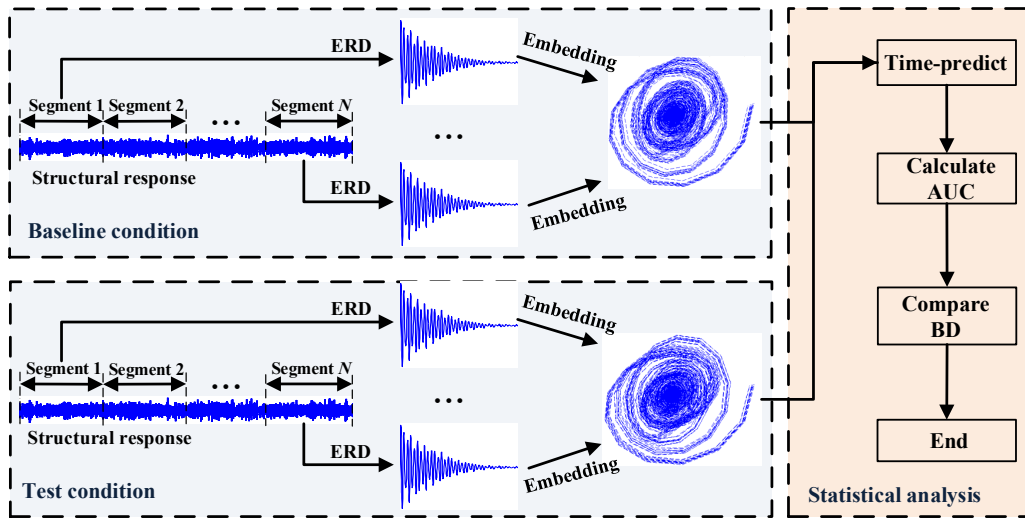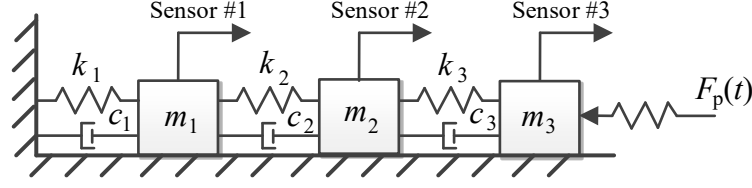

Figure 3. The procedure of the proposed method

4 Numerical simulations

4.1 Computational model set-up

A 3-DOF simulated spring-mass system subject to ambient excitation, as shown in Figure

4, is adopted to validate the proposed method, in which all the structural responses are available analytically.

Figure 4. 3-DOF spring mass system

The mass and stiffness are set to be $m_i=1kg$ and $k_i=2.0\times10^4 N/m$ respectively for all $i=1,2,3$. Rayleigh damping is adopted building matrix C which is proportional damping model to the mass matrix M and stiffness matrix K, i.e., $C=\alpha M +\beta K$. Assuming the damping ratios for the first and third modes of the system are both 0.02, leading to the damping coefficients $\alpha=2.0189$ and $\beta=1.259\times10^{-4}$.

According to the assumption that the non-stationary excitation $f(t)$ is the product of white noise $e(t)$ and an envelope function $h(t)$, as shown in the Appendix. Two types of non-stationary excitations are discussed in this paper. The first one selected is an amplitude modulation (AM) signal, whose envelope function is designed as

$$h_{e1}\left(t,\tau\right)=\begin{cases} e^{-at}-e^{-bt} & \left(\tau=0\right) \\ 0 & \left(\tau>0\right) \end{cases}, \tag{15}$$

where τ denotes time delay, a and b are parameters for the AM function $e^{-at}-e^{-bt}$ and these two stochastic parameters vary in the intervals [0.005,0.015] and [0.015,0.025] respectively. The second type of excitation is AM and frequency modulation (FM) signal, which the envelop function is designed as

$$h_{e2}\left(t,\tau\right)=\left(e^{-at}-e^{-bt}\right)\times e^{-\xi_0\omega_0\tau}\times\sin\left(\omega_0\sqrt{1-\xi_0^2}\,\tau\right), \tag{16}$$

where $\sin(\cdot)$ describes the FM function, in which ξ_0 is bounded in [0.05,0.1] and ω_0 is bounded in $[15\pi,25\pi]$, since most of the natural non-stationary excitation is low frequency, such as seismic waves. The input force $f(t)$ to the system is applied on the right hand side of the structure.

(a)   (b)
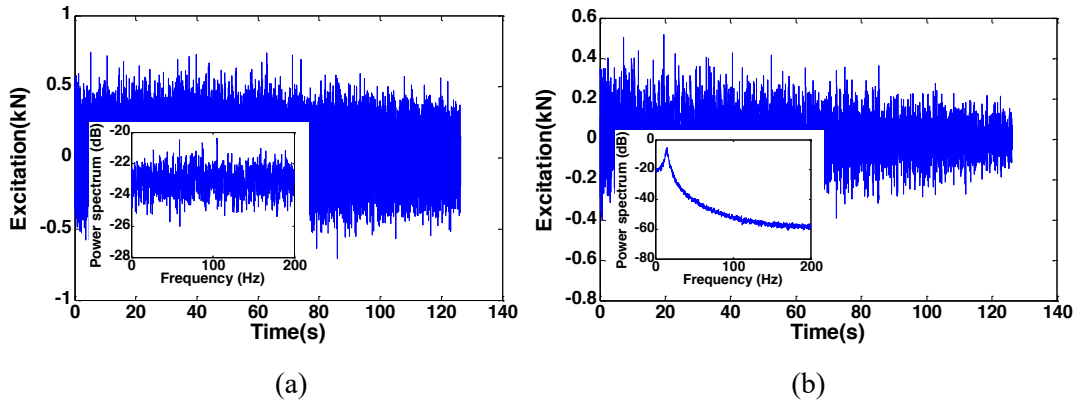
Figure 5. Non-stationary excitation and corresponding power spectrum for (a) AM signal (b) AMFM signal

To consider both linear and nonlinear damages, the spring element k_2 is tuned in two ways:

linear stiffness degradation and nonlinear change to the stiffness governed by

$$k_2^d = (1-\gamma)k_2\left[1 - \mu|x_1 - x_2| + \mu(x_1 - x_2)^2\right], \qquad (17)$$

where superscript d represents damage, γ and μ are linear and nonlinear damage severity coefficient respectively, x_1 and x_2 are the displacement at mass 1 and 2. All damage scenarios are listed in Table 1.

Table 1. Simulation damage scenarios

Damage cases	Case0	Case1	Case2	Case3	Case4	Case5	Case6
γ	0	1%	3%	5%	10%	15%	20%
μ	0.00	0.05	0.10	0.25	0.50	0.75	1.00

When only linear damage condition is considered, the nonlinear coefficient μ is set to be 0 at all damage cases. Simulations are conducted using Newmark's direct integration method, with a 0.01-second time step. Displacement responses at all three masses are calculated, each of which consists 505,000 points and is recorded at a 400 Hz sampling rate. The segment of the first 5000 points is abandoned, and the rest of the time series are divided into 10 segments, with 50,000 points each. Prior to RD technique analysis, each segment is normalized to zero mean and unit standard deviation in order to remove the global signal-to-noise variability and/or excitation amplitude fluctuation.

4.2 Damage detection results

First, linear damage cases are implemented. For random decrement technique, the trigger value A is set to be $1.5\,\sigma_x$ since it is the optimal value for A according to reference [25], and length T is selected as 1 000. After the RD signals from baseline are obtained, AMI and FNN functions are utilized to estimate the optimal embedding lag and dimension. Since the general trend of AMI and FNN functions from all segments are similar, the AMI and FNN values from a sample segment are plotted in Figure 6. AMI reaches the first minimum at lag $T=10$ for all three DOFs, so the appropriate lag is set to be 10. The percentage of FNN function declines rapidly and firstly approaches zero at $M=4$, indicating the signal contains most of information in the first few dimensions.

(a)   (b)
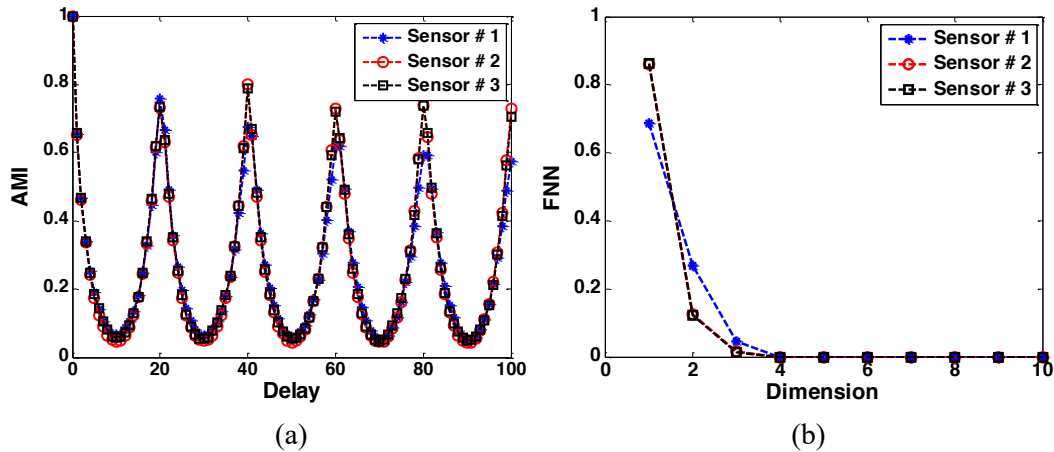
Figure 6. Embedding parameters using displacement response for (a) AMI (b) FNN

Ten trajectories are reconstructed under the same damage scenario using the optimal embedding parameters and overlapped into one phase state. The time prediction error algorithm and bootstrap technique are implemented to compute the distribution of TPEM. Results of this

computation for sensor 1 and sensor 3 are illustrated in Figure 7. It is observed that the distributions shift to the right when there is damage. With more severe damage, the damaged distribution moves farther apart from the baseline (baseline and case 0 both indicate the undamaged condition). Moreover, there is not only mean shift of these distributions, but also the variance change, thus the variance should be considered in the statistical metric for discriminating damages, as proposed in Eq. (14).
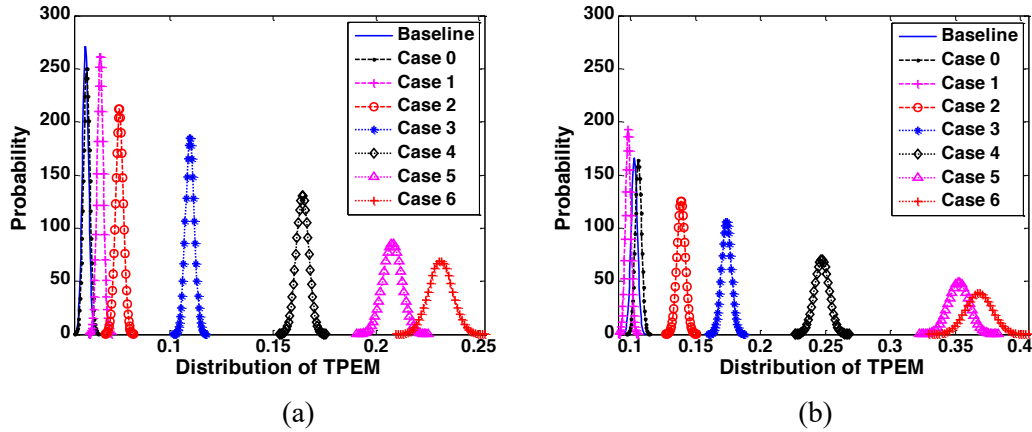

(a)   (b)

Figure 7. Distribution of TPEM for (a) Sensor 1 (b) Sensor 3

Figure 8 depicted the two statistical metrics, namely AUC and BD. From Figure 8-(a), even with 1% of stiffness loss (case 1), the AUCs for all sensors are very close to 1, indicating the proposed method is sensitive and applicable for early damage warning, which is critical for condition-based maintenance scheduling. Figure 8-(b) shows that BD will increase as damage level increases, thus the comparative severity can be inferred from BD plots. The absolute magnitude of damage could be calibrated and identified via a supervised learning procedure, but this procedure is beyond the scope of this study.
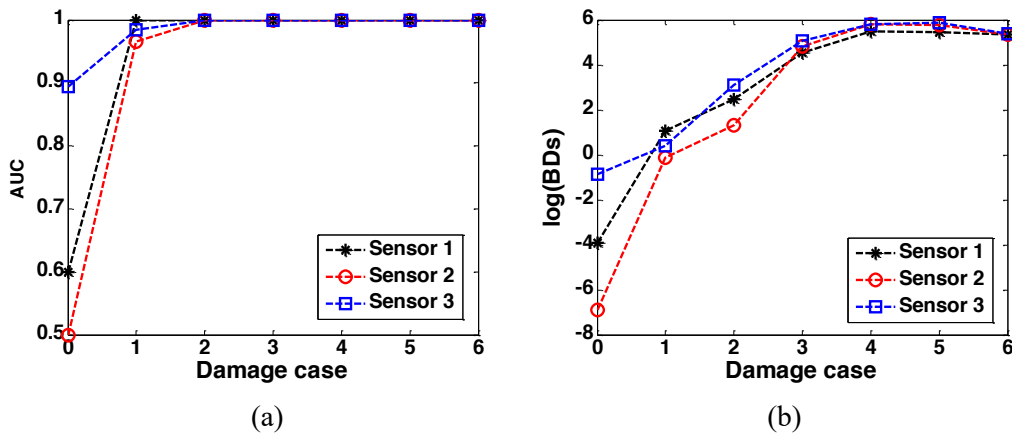

(a)   (b)

**Figure 8.** Statistical metrics under linear damage for (a) AUCs (b) BDs

The results from linear damage cases motivate sufficiently to extend the methodology to nonlinear damage cases. To consider the variability caused by nonlinear damage, the procedure depicted in Figure 3 is repeated for 50 times with different stochastic excitations, the mean values along with the 10th and 90th percentiles of the two metrics are shown in Figure 9, where the mean is located at the intersection between dot line and error bar at each damage case, and the 10th and 90th percentiles are marked with short horizontal line at the end of error bars.

Under low level damages, e.g. case 1 and 2, the range of error bars for AUC expanses widely. This trend is related to the uncertainty caused by nonlinear damage, which can be viewed as noise at some extent; thus the percentiles of AUCs spread widely when the damage severity is small. However, the interval between 10th and 90th percentiles decreases rapidly as damage severity increases, for example, from damage case 3 to 6 (5% stiffness loss in spring k_2 in case 3), the 10th and 90th percentiles almost the same and mean of the AUCs for all sensors approach 1, indicating there is little false positive for detecting the presence of damage in these damage cases. Similarly, the interval of the percentiles of BDs will constrict as damage level deteriorates, the mean of BDs will increase, and thus the damage severity can be identified.

(a)   (b)
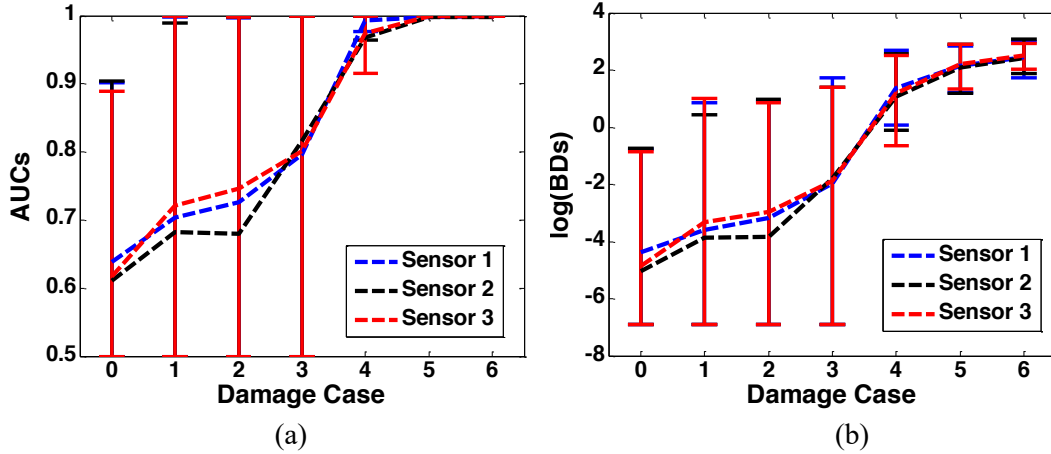
Figure 9. Error bar of nonlinear damage under AM excitation for (a) AUCs (b) BDs

The same procedure is repeated for AMFM excitation and error bars for AUCs and BDs are shown in Figure 10. Although the 10 percentage and 90 percentage of AUCs and BDs for all sensors fluctuate heavier comparing to AM excitation, the average of these two metrics increases monotonically as damage severity increase, indicating that the present and severity of damage under AMFM excitation can be nicely identified.

(a)   (b)
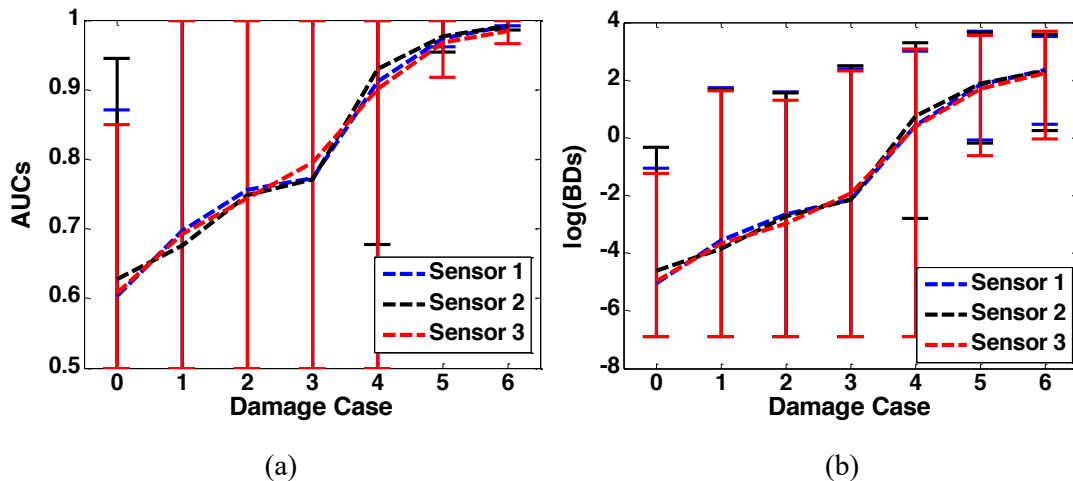
Figure 10. Error bar of nonlinear damage under AMFM excitation for (a) AUCs (b) BDs

4.3 Effect of noise

To validate the proposed method in a more rigorous test, the AM time history measurements under linear damage are artificially contaminated by different levels of white

noise (uncorrelated with the input), and then BDs are calculated for sensor 1 and 3 for the sake of brevity. The results clearly indicate the deterioration of damage identification performance with increasing levels of noise, especially when loss of stiffness is below 5% (case 1 to case 3). However, at relatively high damage severity, e.g. above 10%, the BDs under different noise level just vary around the noise-free value, indicating that the damage-induced change dominates the detection rather than noise. However, the detection capability saturates when the damage is severe, because the damage induced nonlinearity causes significant variance that dominates the BD compared to the mean shift, and thus growing damages (shifting of mean) may not increase BD as it used to. Nonetheless, for small damages, the results demonstrate a monotonically increasing BD, even with moderate amount of noise contamination, indicating the capability of severity evaluation.

<table>
<tr><td>(a)</td><td>(b)</td></tr>
</table>
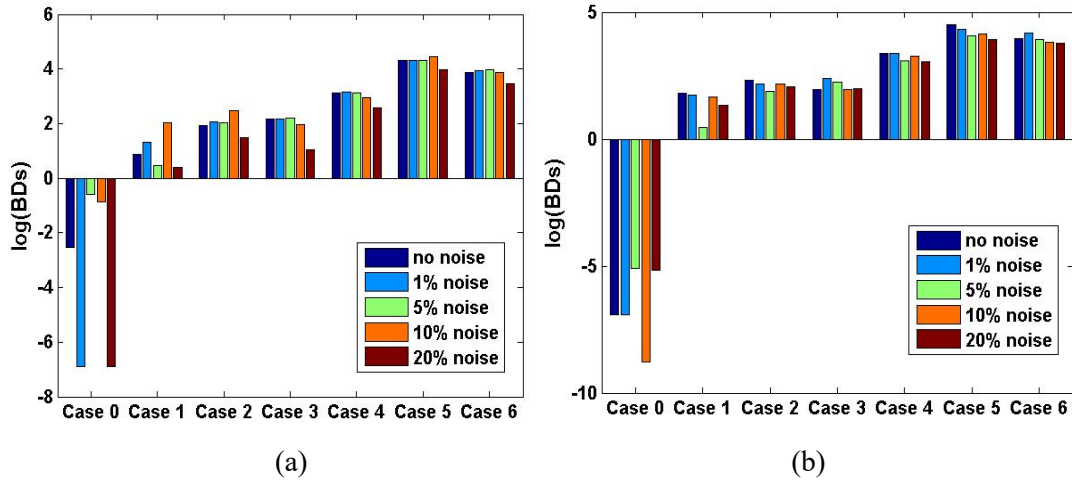
Figure 11. BDs under different noise level for (a) sensor 1 (b) sensor 3

5 Experimental verification

5.1 Test description

Theoretically, the ERD technique can only applied to deal with linear signals/damages, but it has been successfully extended for nonlinear systems by previous researches[17, 18], and promising results have obtained from the numerical simulation early in this paper. Capabilities of identifying nonlinear damages of the proposed method are further investigated using a more complex and realistic structure. A four-story and one-bay plane steel frame is used as a damage detection test-bed shown in Figure 12. The size of components is 350×65×4mm and components are connected via steel angle brackets using two bolts. The base is a 12mm thick steel plate in order to separate the unmeasured excitations. A shaker is connected to the structure by a stinger connected to the column at the first floor. A commercial input signal deviser and conditioner by Spectrum company are used to send the AMFM waveform, which is designed according to Eq.(16), to the shaker. Damage is introduced by removing bolts at the connection A as shown in Figure 12. The damage scenarios are listed in Table 4. Four ICP accelerometers are deployed at the joint between the column and the beam. The nominal sensitivity of each accelerometer is $100mVg^{-1}$. 505 000 data points are measured for each accelerometer under each case with 500Hz sampling rate. The segment of first 5 000 points is abandoned, and the rest of the time series are divided into 10 segments, with 50 000 points each. Prior to ERD technique analysis, each segment is normalized to zero mean and unit standard deviation in

order to remove the global signal-to-noise variability and/or excitation amplitude fluctuation.

(a)   (b)
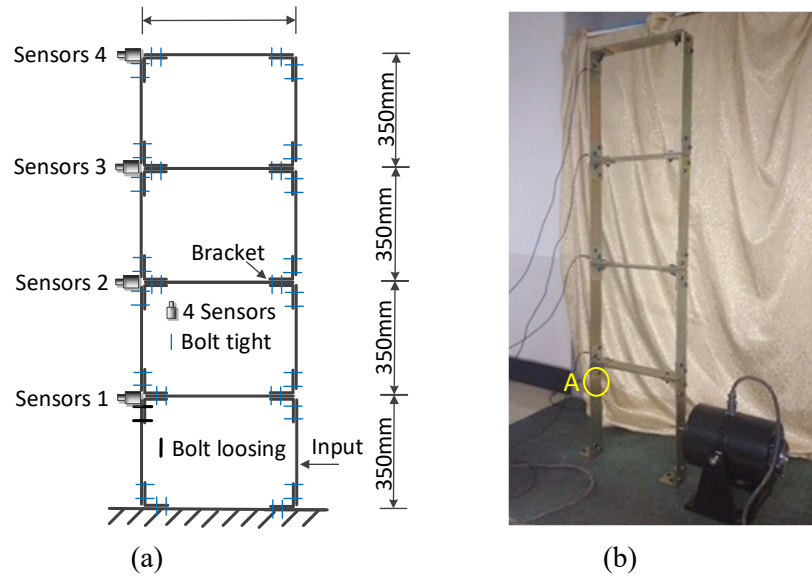
**Figure 12.** Description of the four-story test-bed structure: (a) sketch (b) photo

Table 4. Three damage cases

Damage case	0	1	2	3
Description	Baseline	One bolt loosened	The second bolt finger tight	Two bolts loosened

5.2 Damage detection results

The data measured from healthy condition need to be split into baseline and reference to get BD and AUC value when the system is under healthy condition. To that end, the 20 recorded acceleration segments under healthy condition are divided into baseline and reference data sets, each set with 10 segments.

The RD technique is adopted, in which the trigger value A and length P are chosen as 1.5 σ_x and 1 000 respectively, and then the transient trajectories are reconstructed and plotted in an overlapped fashion. Figure 13 illustrates the RD signals and corresponding trajectory construction at sensor 4. It shows that the overlapped trajectories are a width-limited stripe evolving from the initial conditions to zero.


(a)   (b)
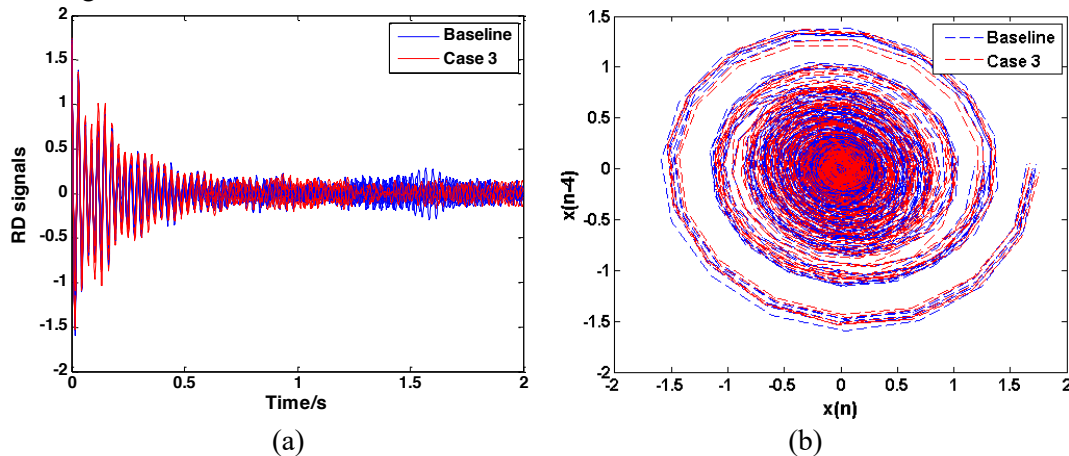
**Figure 13.** RD technique and trajectories under AMFM excitation (a) RD signals (b) phase

The probability density functions of TPEMs, which are showed in Figure 14, are acquired using time prediction error algorithm. As can be seen in these graphs, larger deviation from healthy scenario in general indicates larger damage, and both the mean and variance of the random variable vary as damage amplitude increase, therefore BD in Eq. (6) is adopted in an effort to statistically discriminate the amount of deviation.

(a)   (b)
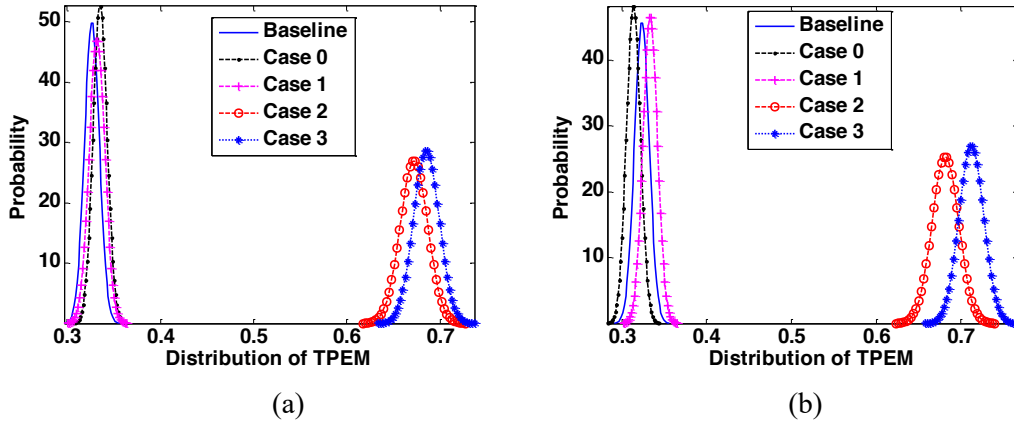
Figure 14. Distribution of the prediction error mean for (a) Sensor 2 (b) Sensor 4

The AUCs and BDs for the reconstructed phase state are plotted in Figure 15. Even in damage case 1, only the value of AUC for sensor 1 and sensor 2 under 0.8, all other values are 1, indicating that the damage present can be detected to some extent. Furthermore, the BDs will increase as the damage level increase. This implies that the damage severity can be identified successfully.

(a)   (b)
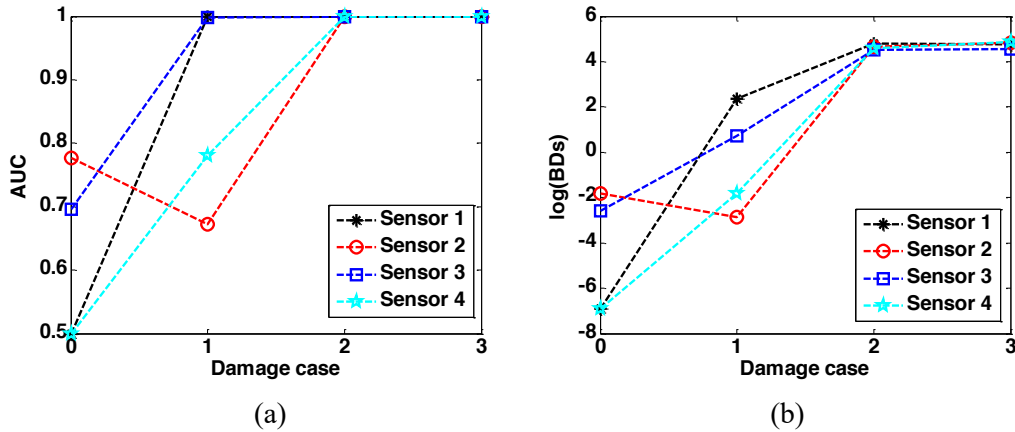
Figure 15. Statistic metrics for (a) AUCs (b) BDs

6 Conclusion

A transient phase-state-based damage detection method under non-stationary ambient excitation is introduced in this study. The method is based on the fact that the transient trajectories, reconstructed from free decay response with non-stationary excitation, would explore variation in structural dynamics caused by damages, just like the attractor embedded from the steady-state response under deterministic excitation. The random decrement technique

is extended to extract the free decay response from the non-stationary response, and trajectories reconstructed from different data segments are overlapped into the phase space in order to have sufficient realizations for statistical analysis. Time prediction error algorithm is employed to obtain the damage feature and then the area under ROC curve and the Bhattacharyya distance are utilized as statistical metrics to identify presence and severity of the damage respectively.

A 3-DOF mass spring numerical system and a lab-scale structure with different nonlinear damage magnitude are utilized to validate the damage identification performance of the proposed method. Results from the computational system show that the presence and severity of damages are accurately identified. Although noise degrades the accuracy, compelling results are obtained as damage level increases. Results from the experiment indicate that the proposed method can be extended for nonlinear damage identification as well.

The transient phase space based method shows promising performance of damage identification and further study will be focused upon in-situ factors influence analysis, including real operational and environmental uncertainties.

Acknowledgement

Appendix

In order to extend the RD technique for non-stationary excitation, the statistical characteristics of the non-stationary excitation need to be considered. According to the evolutionary spectrum theory[26], the non-stationary ambient excitation f may be viewed as non-stationary white noise in the form of a convolution model. In other words, the white noise e is filtered by a time-vary linear system,

$$f(t_k) = \sum_{\tau=0}^{p} h_e(t_k, \tau) e(t_k - \tau), \tag{a.1}$$

where $h_e(t_k, \tau)$ is the impulse response function of the linear system with time delay τ, p denotes the maximum time delay step and t_k represents the k-th time point using interval sampling strategy.

Due to the statistical independence of the white noise e, the mean and variance of the non-stationary ambient excitation f can be written respectively as

$$\begin{aligned} E(f(t_k)) &= \sum_{\tau=0}^{p} h_e(t_k, \tau) E(e(t_k - \tau)) = 0 \\ D(f(t_k)) &= \sum_{\tau=0}^{p} h_e^2(t_k, \tau) D(e(t_k - \tau)) = \sigma_e^2 \sum_{\tau=0}^{p} h_e^2(t_k, \tau) \end{aligned}, \tag{a.2}$$

where σ_e denotes the variance of the white noise.

If the excitation f is divided into N segments with length p, all segments are averaged as

$$F(p) = \frac{1}{N} \sum_{l=1}^{N} f(t_l + p), \tag{a.3}$$

where the subscript l is the starting time step of the l-th segments. Considering the Eq. (a.2) and Eq. (a.3), the mean of the averaged $F(p)$ can be deduced as

$$E\big(F(p)\big) = \frac{1}{N}\sum_{l=1}^{N}\sum_{\tau=0}^{p} h_e(t_l+p,\tau)E\big(e(t_l+p-\tau)\big) = 0. \tag{a.4}$$

Eq. (a.4) shows that the mean of $F(p)$ for the non-stationary ambient excitation is zero. And via the same procedure, the variance of the signature $F(p)$ can be obtained as

$$D\big(F(p)\big) = \frac{1}{N^2}\sum_{l=1}^{N}\sum_{\tau=0}^{p} h_e^2(t_l+p,\tau)D\big(e(t_l+p-\tau)\big) = \frac{\sigma_e^2}{N^2}\sum_{l=1}^{N}\sum_{\tau=0}^{p} h_e^2(t_l+p,\tau) + \frac{\operatorname{cov} f}{N^2}, \tag{a.5}$$

where

$$\operatorname{cov} f = 2\sum_{l=1}^{N-1}\sum_{i=l+1}^{N} \operatorname{cov}\big(f(t_l+p), f(t_i+p)\big). \tag{a.6}$$

Substituting Eq. (a.1) into Eq. (a.6),

$$\operatorname{cov} f = 2\sigma_e^2\sum_{l=1}^{N-1}\sum_{i=l+1}^{N}\sum_{\tau=0}^{p} h_e(t_l+p,\tau)h_e(t_l+p,t_i-t_l+\tau). \tag{a.7}$$

Substituting Eq. (a.7) into Eq. (a.5), the variance of signature $F(p)$ can be expressed as,

$$D\big(F(p)\big) = \frac{\sigma_e^2}{N^2}\sum_{l=1}^{N}\sum_{\tau=0}^{p} h_e^2(t_l+p,\tau) + \frac{2\sigma_e^2}{N^2}\sum_{l=1}^{N-1}\sum_{i=l+1}^{N}\sum_{\tau=0}^{p} h_e(t_l+p,\tau)h_e(t_l,t_i-t_l+\tau). \tag{a.8}$$

From Eq. (a.8), we know that the variance depends on the impulse response function, that is, the variance rests with the type of the non-stationary ambient excitation.

(1) White noise amplitude excitation

If the excitation can be modeled as white noise amplitude signal, which is a product of white noise with a time-independent function satisfying the following conditions,

$$h_e(t_l+p,\tau) = \begin{cases} W(t_l+p) & (\tau=0) \\ 0 & (\tau>0) \end{cases} \quad \text{for all } l, \tag{a.9}$$

where $W(t_l)$ is the modulation function. Substituting Eq.(a.9) into Eq.(a.8), there is

$$D\big(F(p)\big) = \frac{\sigma_e^2}{N^2}\sum_{l=1}^{N} W^2(t_l+p). \tag{a.10}$$

(2) The correlation amplitude excitation

When the impulse response function $h_e(t_l,\tau)$ is time-variant, the non-stationary excitation, called the correlation amplitude signal, will vary with time, such as the vehicle loadings, seismic waves and fluctuating wind excitation. Assuming that the period between t_l and t_{l+1} in Eq. (a.3) is much greater than the decay period of the impulse response function, i.e.,

$$\left| \sum_{i=l+1}^{N} h_e(t_l+p,t_i-t_l+\tau) \right| \ll h_e(t_l+p,\tau). \tag{a.11}$$

Note the second term in Eq.(a.8) is much smaller than the first term under aforementioned assumption. Therefore, Eq. (a.8) can be rewritten as:

$$D\big(F(p)\big) = \frac{\sigma_e^2}{N^2} \sum_{l=1}^{N} \sum_{\tau=0}^{p} h_e^2(t_l + p, \tau). \qquad\qquad (a.12)$$

The preceding results indicate that the mean of the non-stationary excitation is zero and the variance of randomdec signal will decrease quadratic with the superimposed times N, given that the non-stationary excitation can be represented by a product of white noise with an envelope function.

References

[1]   C. R. Farrar and K. Worden, "An introduction to structural health monitoring," *Philosophical Transactions of the Royal Society A: Mathematical, Physical and Engineering Sciences,* vol. 365, pp. 303-315, 2007.

[2]   K. Danai, S. A. Civjan, and M. M. Styckiewicz, "Direct method of damage localization for civil structures via shape comparison of dynamic response measurements," *Computers & Structures,* vol. 92, pp. 297-307, 2012.

[3]   B. Jaishi and W.-X. Ren, "Finite element model updating based on eigenvalue and strain energy residuals using multiobjective optimisation technique," *Mechanical Systems and Signal Processing,* vol. 21, pp. 2295-2317, 2007.

[4]   H. Sohn and C. R. Farrar, "Damage diagnosis using time series analysis of vibration signals," *Smart materials and structures,* vol. 10, p. 446, 2001.

[5]   J. Nichols, C. Nichols, M. Todd, M. Seaver, S. Trickey, and L. Virgin, "Use of data-driven phase space models in assessing the strength of a bolted connection in a composite beam," *Smart Materials and Structures,* vol. 13, p. 241, 2004.

[6]   L. Moniz, J. Nichols, C. Nichols, M. Seaver, S. Trickey, M. Todd*, et al.*, "A multivariate, attractor-based approach to structural health monitoring," *Journal of Sound and Vibration,* vol. 283, pp. 295-310, 2005.

[7]   J. Nichols, M. Todd, and J. Wait, "Using state space predictive modeling with chaotic interrogation in detecting joint preload loss in a frame structure experiment," *Smart Materials and Structures,* vol. 12, p. 580, 2003.

[8]   L. Overbey and M. Todd, "Damage assessment using generalized state-space correlation features," *Structural Health Monitoring,* vol. 7, pp. 347-363, 2008.

[9]   I. Trendafilova and E. Manoach, "Vibration-based damage detection in plates by using time series analysis," *Mechanical Systems and Signal Processing,* vol. 22, pp. 1092-1106, 2008.

[10]   M. Todd, J. Nichols, L. Pecora, and L. Virgin, "Vibration-based damage assessment utilizing state space geometry changes: local attractor variance ratio," *Smart Materials and Structures,* vol. 10, p. 1000, 2001.

[11]   K. Worden, C. R. Farrar, J. Haywood, and M. Todd, "A review of nonlinear dynamics applications to structural health monitoring," *Structural Control and Health Monitoring,* vol. 15, pp. 540-567, 2008.

[12]   J. Nichols, "Structural health monitoring of offshore structures using ambient excitation," *Applied ocean research,* vol. 25, pp. 101-114, 2003.

[13]   L. Overbey, C. Olson, and M. Todd, "A parametric investigation of state-space-based prediction error methods with stochastic excitation for structural health monitoring," *Smart Materials and Structures,* vol. 16, p. 1621, 2007.

[14]   G. Liu, Z. Mao, M. Todd, and Z. Huang, "Localization of nonlinear damage using state-space-based predictions under stochastic excitation," *Smart Materials and Structures,* vol. 23, pp. 25-36, 2014.

[15]   G. Liu, Z. Mao, M. D. Todd, and Z. Huang, "Damage Assessment with State-Space Embedding Strategy and Singular Value Decomposition under Stochastic Excitation," *Structural Health Monitoring,* vol. 13, pp. 131-142, 2013.

[16]   A. A. Elshafey, M. R. Haddara, and H. Marzouk, "Identification of the excitation and reaction forces on offshore platforms using the random decrement technique," *Ocean Engineering,* vol. 36, pp. 521-528, 2009.

[17]   O. V. Shiryayev and J. C. Slater, "Improved structural damage identification using random decrement signatures: Application to FEM data," *Structural Control and Health Monitoring,* vol. 15, pp. 1006-1020, 2008.

[18]   A. B. Mahfouz, "Identification of the nonlinear ship rolling motion equation using the measured response at sea," *Ocean Engineering,* vol. 31, pp. 2139-2156, 2004.

[19]   O. V. Shiryayev and J. C. Slater, "Application of the random decrement technique to nonlinear dynamic systems," in *Proceedings of the 47th AIAA/ASME/ASCE/AHS/ASC Structures, Structural Dynamics, and Materials Conference*, 2006.

[20]   F. Takens, "Detecting strange attractors in turbulence," in *Dynamical systems and turbulence, Warwick 1980*, ed: Springer, 1981, pp. 366-381.

[21]   A. M. Fraser and H. L. Swinney, "Independent coordinates for strange attractors from mutual information," *Physical review A,* vol. 33, p. 1134, 1986.

[22]   M. B. Kennel, R. Brown, and H. D. Abarbanel, "Determining embedding dimension for phase-space reconstruction using a geometrical construction," *Physical review A,* vol. 45, p. 3403, 1992.

[23]   B. Efron and R. Tibshirani, *An introduction to the bootstrap* vol. 57: Chapman & Hall/CRC, 1993.

[24]   E. Choi and C. Lee, "Feature extraction based on the Bhattacharyya distance," *Pattern Recognition,* vol. 36, pp. 1703-1709, 8// 2003.

[25]   J. C. Asmussen, "Modal analysis based on the random decrement technique: application to civil engineering structures," unknown, 1997.

[26]   P. M. B, "Power spectral analysis of non-stationary random processes," *Journal of Sound and Vibration,* vol. 6, pp. 86-97, 1967.